Structural Engineering and Mechanics, Vol. 21, No. 3 (2005) 315-332
DOI: http://dx.doi.org/10.12989/sem.2005.21.3.315

A Moving Least Squares weighting function for the Element-free Galerkin Method which almost fulfills essential boundary conditions

Thomas Most† and Christian Bucher‡

Institute of Structural Mechanics, Bauhaus-University, Weimar, Marienstr. 15, D-99423 Weimar, Germany

(Received November 2, 2004, Accepted July 26, 2005)

Abstract. The Element-free Galerkin Method has become a very popular tool for the simulation of mechanical problems with moving boundaries. The internally applied Moving Least Squares interpolation uses in general Gaussian or cubic weighting functions and has compact support. Due to the approximative character of this interpolation the obtained shape functions do not fulfill the interpolation conditions, which causes additional numerical effort for the application of the boundary conditions. In this paper a new weighting function is presented, which was designed for meshless shape functions to fulfill these essential conditions with very high accuracy without any additional effort. Furthermore this interpolation gives much more stable results for varying size of the influence radius and for strongly distorted nodal arrangements than existing weighting function types.

Key words: interpolation; Moving Least Squares; meshless discretization; boundary conditions.

1. Introduction

In the recent years meshless methods (Belytschko *et al*. 1996) have been developed for mechanical problems with growth of surfaces, such as in crack propagation. By using meshless methods for these purposes no complex mesh generators are necessary and a state variable transfer, if it is required, is straightforward due to the mainly continuous stress functions. One of the most common meshless methods is the Element-free Galerkin Method (EFG) (Belytschko *et al*. 1994), which uses the Moving Least Squares (MLS) procedure (Lancaster and Salkauskas 1981) for the interpolation of the displacement function. An adaptive coupling (Karutz 2000) of meshless zones with traditional finite elements seems to be necessary to obtain an efficient algorithm, because of the larger numerical effort of the meshless methods to determine the shape function values. Due to the approximative character of the MLS interpolation using standard weighting functions the interpolation condition and the essential boundary conditions are not fulfilled automatically. Therefore a direct coupling with finite elements is not straightforward. Different methods have been developed to overcome this problem, such as the application of Lagrange multipliers (Belytschko *et al*. 1994), the introduction of a penalty term (Häussler-Combe 2001) or the usage of special

† Research Associate, Corresponding author, E-mail: thomas.most@uni-weimar.de
‡ Professor

boundary components (Belytschko *et al.* 1995, Karutz 2000). By using Lagrange multipliers, the system of equations, which has to be solved, becomes larger and special solvers are required due to the singularity of the coefficient matrix. The penalty solution can force fulfillment of the boundary conditions only approximately and the correct choice of the penalty term is difficult. The formulation of boundary components fulfills the boundary conditions but is very un-practical for the adaptive coupling with finite elements. While all three methods, which require additional numerical effort, fulfill the boundary conditions with a sufficient accuracy, the interpolation conditions for the internal nodes are not satisfied. For the application of the MLS interpolation in the Moving Least Squares Differential Quadrature Method (Liew *et al.* 2003a) the boundary conditions are considered directly by means of additional equations (Liew *et al.* 2003b, 2004). This is similar to the application of Lagrange multiplier in the Element-free Galerkin Method, but with less additional effort. Nevertheless the interpolation condition is again not fulfilled at every node, which may lead to a strong dependence of the calculated displacement and stress values on the specified influence radius of the weighting function.

For all of these reasons the authors designed a new regularized weighting function which fulfills the interpolation and boundary conditions automatically with very high accuracy. This leads to an easy application within a Galerkin approach similar to the finite element interpolation or the Natural Neighbor Interpolation (Sukumar *et al.* 1998). The numerical effort for the computation of the weighting function values is similar than for standard MLS weighting functions and furthermore no additional effort is necessary to apply geometrical boundary conditions. Thus one of the main problems for the application of the MLS interpolation in a Galerkin scheme is solved with this new weighting type. The properties of the meshless shape functions obtained with this regularized weighting function are almost independent of the influence radius size. This leads to very stable results which will be shown for several numerical examples.

For the computation of the system matrices and vectors within a Galerkin method the integration over the domain is necessary. In general this integration is carried out by using background cells (Belytschko *et al.* 1996). Due to the fact, that the integration cells do not coincide with the influence domain of the nodes, this integration is not exact and a large number of integration points is necessary to represent the displacement field with sufficient accuracy. Another integration approach is a nodal integration scheme based on an assumed strain method. This method was proposed by (Chen *et al.* 2001) for the Element-free Galerkin Method and can reproduce a linear displacement field exactly. The method uses a Voronoi diagram for defining integration cells, whereby a representative strain at each node is determined by observing the integration constraints for a constant stress state. In (Unger *et al.* 2004) it was shown, that this method fails for systems with load or geometry induced singularity points, like crack tips, which can be observed from an artificial oscillation of the displacements. Because of these reasons the authors decided to use triangular background cells spanned by three nodes for the numerical integration (Most and Bucher 2003, Most *et al.* 2004b). These cells are computed with the Delaunay triangulator "Triangle" (Shewchuk 1996). The integration over boundary lines does not cause any problems, due to the fact, that the boundary segments coincide with the triangle edges.

2. Moving Least Squares interpolation

If an arbitrary function u is interpolated by using a polynomial the following formulation can be

obtained at a point **x**

$$u(\mathbf{x}) = (1 \;\; x \;\; y \;\; xy \;\; x^2 \;\; y^2 \;\; \ldots) \begin{bmatrix} a_1 \\ \vdots \\ a_n \end{bmatrix} = \mathbf{p}^T(\mathbf{x})\mathbf{a} \tag{1}$$

where $\mathbf{p}(\mathbf{x})$ is the base vector and $\mathbf{a}$ contains the coefficients of the polynomial. These coefficients are constant in the interpolation domain and can be determined directly for some special cases if the number of supporting points m used for the interpolation is equivalent to the number of coefficients n. This principle is applied for example in the Finite Element Method, where an element-wise interpolation is realized. There the coefficients are simply given as

$$\mathbf{a} = \mathbf{P}^{T^{-1}} \tilde{\mathbf{u}} \tag{2}$$

where $\tilde{\mathbf{u}}$ contains the values of the interpolated function u at the supporting points

$$\tilde{\mathbf{u}} = (u_1 \cdots u_m) \tag{3}$$

and $\mathbf{P}$ consists of the evaluations of the base polynomial at the supporting points

$$\mathbf{P} = (\mathbf{p}_1 \;\; \cdots \;\; \mathbf{p}_m) = \begin{bmatrix} p_1(\mathbf{x}_1) & p_1(\mathbf{x}_2) & \cdots & p_1(\mathbf{x}_m) \\ p_2(\mathbf{x}_1) & p_2(\mathbf{x}_2) & \cdots & p_2(\mathbf{x}_m) \\ \vdots & \vdots & \ddots & \vdots \\ p_n(\mathbf{x}_1) & p_n(\mathbf{x}_2) & \cdots & p_n(\mathbf{x}_m) \end{bmatrix} \tag{4}$$

Within the "Moving Least Squares" (MLS) interpolation method (Lancaster and Salkauskas 1981) the number of supporting points m exceeds the number of coefficients n, which leads to an overdetermined system of equations. This kind of optimization problem can be solved by using a least squares approach

$$\mathbf{P}\tilde{\mathbf{u}} = \mathbf{P}\mathbf{P}^T\mathbf{a}(\mathbf{x}) \tag{5}$$

with changing ("moving") coefficients $\mathbf{a}(\mathbf{x})$. For the accuracy and efficency of a numerical method with internal interpolation of global variables the compact support of the interpolation is essential. This was introduced for the MLS-interpolation by a distance depending weighting function

$$w(d) = \begin{cases} w_g(d) & d \le D \\ 0 & d > D \end{cases} \tag{6}$$

where d is the distance between the interpolation point and the considered supporting point

$$d_i = \|\mathbf{x} - \mathbf{x}_i\| \tag{7}$$

and D is the influence radius, which is introduced as a numerical parameter. As weighting function w all types of functions can be used, which vanish beyond a certain distance equivalent to D and which are positive in the influence domain of a supporting point.

Eq. (5) is expanded to the following formulation

$$\mathbf{B}(\mathbf{x})\tilde{\mathbf{u}} = \mathbf{A}(\mathbf{x})^T\mathbf{a}(\mathbf{x}) \tag{8}$$

where $\mathbf{A}(\mathbf{x})$ and $\mathbf{B}(\mathbf{x})$ are given as

$$\begin{aligned}\mathbf{A}(\mathbf{x}) &= \mathbf{P}\mathbf{W}(\mathbf{x})\mathbf{P}^T \\ \mathbf{B}(\mathbf{x}) &= \mathbf{P}\mathbf{W}(\mathbf{x})\end{aligned} \tag{9}$$

and the diagonal matrix $\mathbf{W}(\mathbf{x})$ can be determined as follows

$$\mathbf{W}(\mathbf{x}) = \mathrm{diag}(w(d_1), \cdots, w(d_m)) \tag{10}$$

where $w(d_1), \cdots, w(d_m)$ are the weighting function values belonging to the supporting points.

The interpolated value of the function u at $\mathbf{x}$ can be obtained by introducing the MLS shape functions

$$u(\mathbf{x}) = \Phi^{MLS}(\mathbf{x})\tilde{\mathbf{u}}\,, \quad \Phi^{MLS}(\mathbf{x}) = \mathbf{p}^T(\mathbf{x})\mathbf{A}(\mathbf{x})^{-1}\mathbf{B}(\mathbf{x}) \tag{11}$$

In contrast to the Finite Element Method the MLS interpolation does not pass through the nodal values. This is due to the applied least squares approach. This implies that the interpolation condition is not fulfilled

$$\Phi_i^{MLS}(\mathbf{x}_j) \neq \delta_{ij} \tag{12}$$

The properties of the MLS interpolation depend mainly on the base polynomial and on the weighting function. This means that functions of polynomial type can be reproduced exactly if the base polynomial has the same order as the interpolated function. Thus the so-called linear completeness, which is necessary for the convergence of a Galerkin method, can be obtained by using a linear base polynomial. The continuity of the MLS interpolation is only influenced by the continuity of the weighting function, if the weighting function has C^k continuity the interpolation has C^k continuity as well.

If the MLS interpolation is applied in a Galerkin approach the interpolated functions are in general the displacements in one, two or three dimensions. For a standard solution procedure the first derivatives of the displacements, the strains, have to be computed. From Eq. (11) the derivatives can be obtained as

$$\frac{\partial u(\mathbf{x})}{\partial x_i} = \left(\frac{\partial \mathbf{p}^T}{\partial x_i}\mathbf{A}^{-1}\mathbf{B} + \mathbf{p}^T\frac{\partial \mathbf{A}^{-1}}{\partial x_i}\mathbf{B} + \mathbf{p}^T\mathbf{A}^{-1}\frac{\partial \mathbf{B}}{\partial x_i}\right)\tilde{\mathbf{u}} \tag{13}$$

where

$$\frac{\partial \mathbf{A}^{-1}}{\partial x_i} = -\mathbf{A}^{-1}\frac{\partial \mathbf{A}}{\partial x_i}\mathbf{A}^{-1}$$
$$\frac{\partial \mathbf{A}}{\partial x_i} = \mathbf{P}\frac{\partial \mathbf{W}}{\partial x_i}\mathbf{P}^T \tag{14}$$
$$\frac{\partial \mathbf{B}}{\partial x_i} = \mathbf{P}\frac{\partial \mathbf{W}}{\partial x_i}$$

Higher order derivatives can be computed in closed form as well. The second derivatives, which might be necessary for adaptive algorithms by using strain gradients, are given as

$$\begin{aligned}\frac{\partial^2 u(\mathbf{x})}{\partial x_i \partial x_j} = \Bigg[& \frac{\partial^2 \mathbf{p}^T}{\partial x_i \partial x_j}\mathbf{A}^{-1}\mathbf{B} \\ & + \frac{\partial \mathbf{p}^T}{\partial x_i}\left(\frac{\partial \mathbf{A}^{-1}}{\partial x_j}\mathbf{B} + \mathbf{A}^{-1}\frac{\partial \mathbf{B}}{\partial x_j}\right) + \frac{\partial \mathbf{p}^T}{\partial x_j}\left(\frac{\partial \mathbf{A}^{-1}}{\partial x_i}\mathbf{B} + \mathbf{A}^{-1}\frac{\partial \mathbf{B}}{\partial x_i}\right) \\ & + \mathbf{p}^T\left(\frac{\partial^2 \mathbf{A}^{-1}}{\partial x_i \partial x_j}\mathbf{B} + \mathbf{A}^{-1}\frac{\partial^2 \mathbf{B}}{\partial x_i \partial x_j} + \frac{\partial \mathbf{A}^{-1}}{\partial x_i}\frac{\partial \mathbf{B}}{\partial x_j} + \frac{\partial \mathbf{A}^{-1}}{\partial x_j}\frac{\partial \mathbf{B}}{\partial x_i}\right)\Bigg]\tilde{\mathbf{u}}\end{aligned} \tag{15}$$

with

$$\frac{\partial^2 \mathbf{A}^{-1}}{\partial x_i \partial x_j} = -\frac{\partial \mathbf{A}^{-1}}{\partial x_i}\frac{\partial \mathbf{A}}{\partial x_j}\mathbf{A}^{-1} - \mathbf{A}^{-1}\frac{\partial^2 \mathbf{A}}{\partial x_i \partial x_j}\mathbf{A}^{-1} - \mathbf{A}^{-1}\frac{\partial \mathbf{A}}{\partial x_i}\frac{\partial \mathbf{A}^{-1}}{\partial x_j}$$
$$\frac{\partial^2 \mathbf{A}}{\partial x_i \partial x_j} = \mathbf{P}\frac{\partial^2 \mathbf{W}}{\partial x_i \partial x_j}\mathbf{P}^T \tag{16}$$
$$\frac{\partial^2 \mathbf{B}}{\partial x_i \partial x_j} = \mathbf{P}\frac{\partial^2 \mathbf{W}}{\partial x_i \partial x_j}$$

3. Weighting functions

3.1 Common function types

Different types of weighting functions can be found in the literature. One of the most common is the Gaussian weighting function of exponential type, which is given as follows (Häussler-Combe 2001)

$$w_G(d) = \frac{e^{-\left(\frac{d}{\alpha D}\right)^2} - e^{-\frac{1}{\alpha^2}}}{1 - e^{-\frac{1}{\alpha^2}}} \tag{17}$$

The shape parameter α is taken in general as 0.4 (Karutz 2000). In Fig. 1 the Gaussian weighting function is displayed as a function of the standardized distance d/D. The first and second derivatives of the weighting function can be obtained as

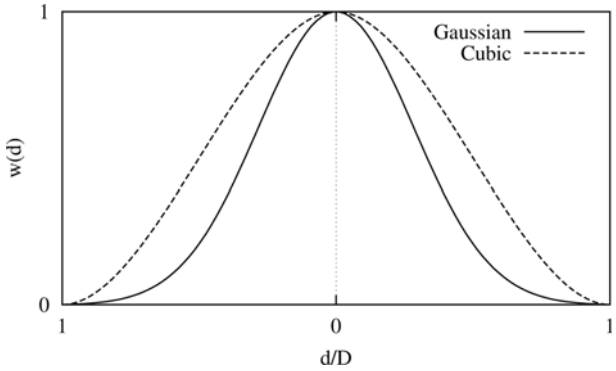

Fig. 1 Gaussian and cubic weighting functions

$$\frac{\partial w_G(d)}{\partial d} = -\frac{e^{-\left(\frac{d}{\alpha D}\right)^2}}{1-e^{-\frac{1}{\alpha^2}}} \cdot \frac{2d}{\alpha^2 D^2}$$
$$\frac{\partial^2 w_G(d)}{\partial^2 d} = -\frac{e^{-\left(\frac{d}{\alpha D}\right)^2}}{1-e^{-\frac{1}{\alpha^2}}} \cdot \left(\frac{2d}{\alpha^2 D^2} - \frac{4d^2}{\alpha^4 D^4}\right) \tag{18}$$

which leads to the following values of the derivatives at the boundary of the influence domain

$$\frac{\partial w_G(d = D; \alpha = 0.4)}{\partial d} \approx 0.024 \frac{1}{D}$$
$$\frac{\partial^2 w_G(d = D; \alpha = 0.4)}{\partial^2 d} \approx 0.278 \frac{1}{D^2} \tag{19}$$

Eq. (19) points out, that C^1 and C^2 continuity can only be reached approximately by using the exponential weighting function type. In Fig. 2 a MLS shape function and its first derivative with respect to x obtained from the Gaussian weighting function is shown for a regular set of nodes.

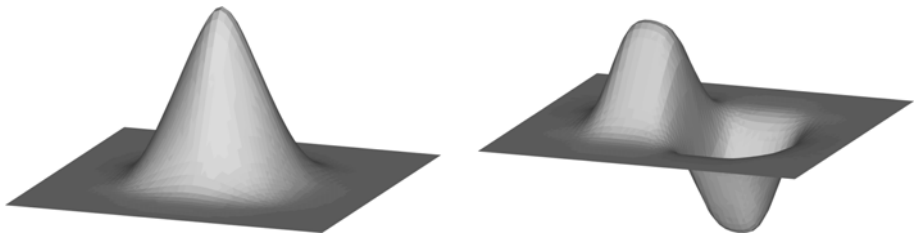

Fig. 2 MLS shape function and first derivative for a regular set of nodes using the Gaussian weighting function

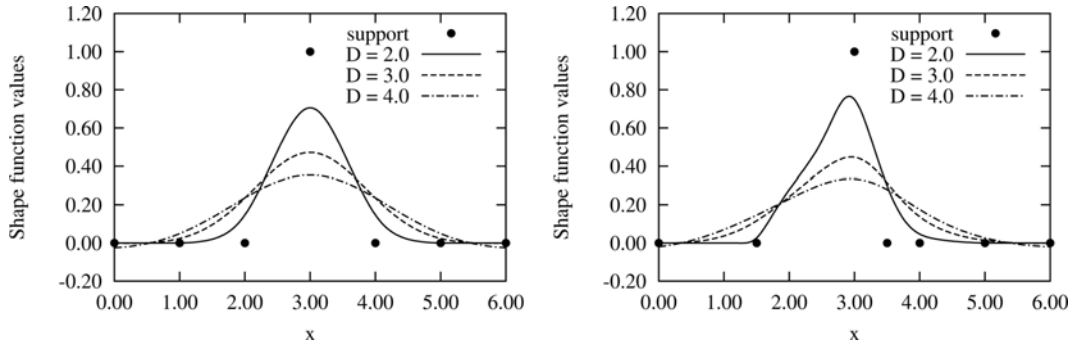

Fig. 3 Nodal shape function of MLS interpolation with Gaussian weighting function and linear base polynomial for regular and irregular sets of nodes

Another standard weighting function is based on a cubic polynomial (Karutz 2000)

$$w_C(d) = 1 - 3\left(\frac{d}{D}\right)^2 + 2\left(\frac{d}{D}\right)^3 \tag{20}$$

and is displayed additionally in Fig. 1.

The derivatives of the cubic weighting function can be determined easily as

$$\begin{aligned} \frac{\partial w_C(d)}{\partial d} &= -\left(\frac{6d}{D^2}\right) + \left(\frac{6d^2}{D^3}\right) \\ \frac{\partial^2 w_C(d)}{\partial^2 d} &= -\left(\frac{6}{D^2}\right) + \left(\frac{12d}{D^3}\right) \end{aligned} \tag{21}$$

which results in the values on the influence boundary given in Eq. (22)

$$\begin{aligned} \frac{\partial w_C(d = D)}{\partial d} &= 0 \\ \frac{\partial^2 w_C(d = D)}{\partial^2 d} &= 6\frac{1}{D^2} \end{aligned} \tag{22}$$

This equation clarifies, that the application of a cubic weighting function leads to an exact C^1 continuous MLS interpolation function.

In Fig. 3 a single nodal shape function of the middle node of a regular set of nodes in $1D$ is shown for increasing influence radius D. As weighting function the above described Gaussian type and a linear base polynomial are used. The figure indicates that with increasing influence radius the shape function error at each support point increases dramatically. This is the main problem for the application of a common weighting function within the MLS interpolation.

3.2 New regularized weighting function

Because of the presented problems using existing weighting function types, the authors decided to

design a new weighting function which allows the fulfillment of the MLS interpolation condition with very high accuracy

$$\Phi_i^{MLS}(\mathbf{x}_j) \approx \delta_{ij} \tag{23}$$

This can only be reached if Eq. (24) is valid

$$w_i(\mathbf{x}_j) \approx \delta_{ij} \tag{24}$$

The weighting function value of a node i at an interpolation point $\mathbf{x}$ is introduced by the following regularized formulation

$$w_R(d_i) = \frac{\tilde{w}_R(d_i)}{\sum_{j=1}^{m} \tilde{w}_R(d_j)} \tag{25}$$

with

$$\tilde{w}_R(d) = \frac{\left(\left(\frac{d}{D}\right)^2 + \varepsilon\right)^{-2} - (1+\varepsilon)^{-2}}{\varepsilon^{-2} - (1+\varepsilon)^{-2}}; \quad \varepsilon << 1 \tag{26}$$

The variable m belongs to the number of supporting points influencing $\mathbf{x}$ and the regularization parameter has to be chosen very small to fulfill Eq. (24) with high accuracy, but it has to be larger than the square root of the machine precision to avoid numerical problems. This limit results from Eq. (26). It is recommended by the authors to use the value

$$\varepsilon = 10^{-5} \tag{27}$$

In Fig. 4 the regularized weighting function is displayed as a function of the standardized distance d/D and the position of the neighbor nodes. The maximum weighting function error at the

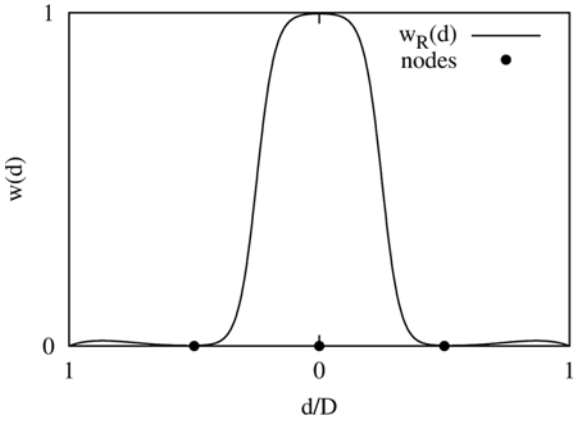

Fig. 4 Regularized weighting function for a single node with two neighbor nodes

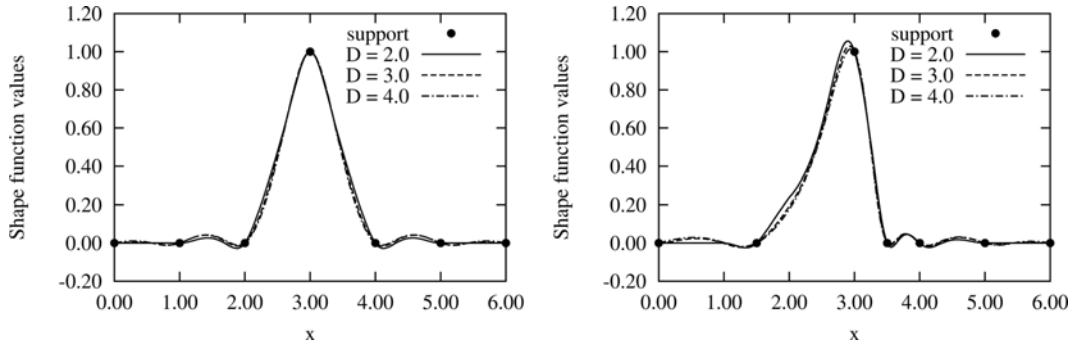

Fig. 5 Nodal shape function of MLS interpolation with regularized weighting function and linear base polynomial for regular and irregular sets of nodes

supporting points can be approximated by assuming

$$\left(\frac{d_{\min}}{D}\right)^2 >> \varepsilon \tag{28}$$

as

$$\left|w_i(\mathbf{x}_j) - \delta_{ij}\right|_{\max} \approx \left(\left(\frac{d_{\min}}{D}\right)^{-4} - 1\right) \cdot \varepsilon^2 \tag{29}$$

where $d_{\min}$ specifies the minimal distance between two nodes.

In Fig. 5 the single nodal shape function by using the regularized weighting function type is shown for different values of the influence radius D.

Fig. 5 and Eq. (29) clearly point out that the interpolation condition is fulfilled with very high accuracy even for irregular sets of nodes with grading node density. In clear contrast to the shape function obtained with the exponential weighting function the influence radius D influences the regularized shape function characteristics marginally if a certain value of D is reached.

In order to reduce the numerical effort for the shape function computation the following simplification of Eq. (25) in combination with Eq. (11) can be made

$$\begin{aligned}
\Phi^{MLS} &= \mathbf{p}^T\mathbf{A}(\mathbf{x})^{-1}\mathbf{B}(\mathbf{x}) \\
&= \mathbf{p}^T[\mathbf{P}\mathbf{W}(\mathbf{x})\mathbf{P}^T]^{-1}\mathbf{P}\mathbf{W}(\mathbf{x}) \\
&= \mathbf{p}^T\left[\frac{1}{\sum_{j=1}^{m}\tilde{w}_R(d_j)}\mathbf{P}\tilde{\mathbf{W}}(\mathbf{x})\mathbf{P}^T\right]^{-1}\frac{1}{\sum_{j=1}^{m}\tilde{w}_R(d_j)}\mathbf{P}\tilde{\mathbf{W}}(\mathbf{x}) \\
&= \mathbf{p}^T[\mathbf{P}\tilde{\mathbf{W}}(\mathbf{x})\mathbf{P}^T]^{-1}\mathbf{P}\tilde{\mathbf{W}}(\mathbf{x})
\end{aligned} \tag{30}$$

This means, that instead of the complex weighting function in Eq. (25) the much simpler

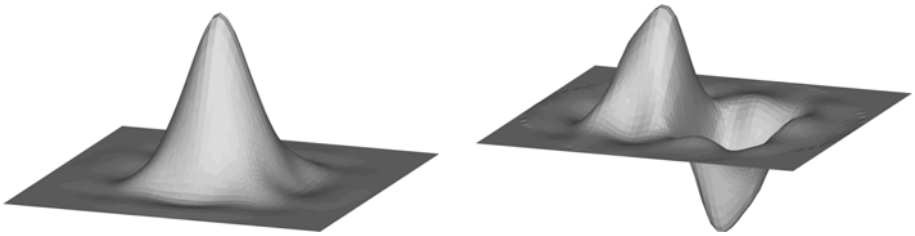

Fig. 6 MLS shape function and first derivative for a regular set of nodes using the regularized weighting function

formulation in Eq. (26) can be used as weighting function by obtaining exactly the same shape function values. The calculation of the first and second derivatives becomes much easier as well

$$\frac{\partial \tilde{w}_R(d)}{\partial d} = -\frac{4d}{D^2}\frac{\left(\left(\frac{d}{D}\right)^2+\varepsilon\right)^{-3}}{\varepsilon^{-2}-(1+\varepsilon)^{-2}}$$
$$\frac{\partial^2 \tilde{w}_R(d)}{\partial^2 d} = \frac{\frac{24d^2}{D^4}\left(\left(\frac{d}{D}\right)^2+\varepsilon\right)^{-4}-\frac{4}{D^2}\left(\left(\frac{d}{D}\right)^2+\varepsilon\right)^{-3}}{\varepsilon^{-2}-(1+\varepsilon)^{-2}} \tag{31}$$

The values on the influence boundary can be approximated as

$$\frac{\partial \tilde{w}_R(d=D)}{\partial d} \approx 4\varepsilon^2\frac{1}{D}$$
$$\frac{\partial^2 \tilde{w}_R(d=D)}{\partial^2 d} \approx 20\varepsilon^2\frac{1}{D^2} \tag{32}$$

Eq. (32) points out, that the derivatives of the regularized weighting function vanish on the boundary of the influence domain, which clarifies the fact, that the application of the presented weighting type leads to an interpolation which show C^1 and C^2 continuity approximately. In Fig. 6 a MLS shape function with corresponding first derivative with respect to x by using the regularized weighting function is shown for a regular set of nodes.

4. Examples

4.1 Shape functions for regular and irregular sets of nodes

Within this example the interpolation errors are calculated for a regular and a irregular set of 5×5 nodes with a distance of $a = 0.25$ m by using the Gaussian and the regularized weighting function. In Fig. 7 both investigated nodal sets are displayed.

First the numerical error according to Eq. (23) at the supporting points for the shape function of

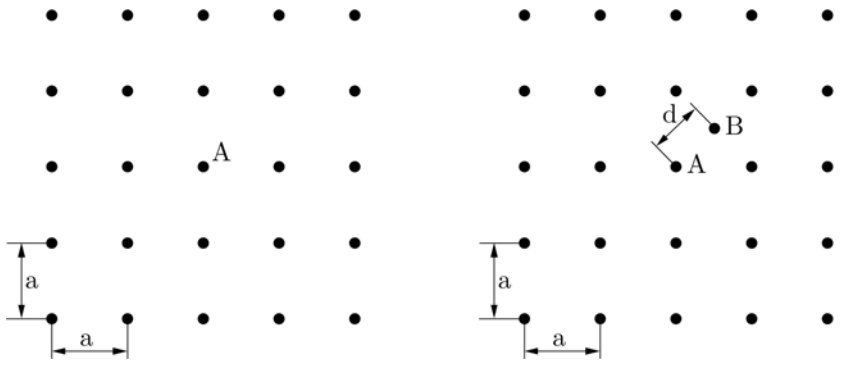

Fig. 7 Investigated regular and irregular set of nodes

node A is analyzed for a varying influence radius D using the regular nodal set. The regularization term is assumed to be $\varepsilon = 10^{-5}$ and the Gaussian shape parameter is taken with $\alpha = 0.3295$. In Table 1 the obtained maximum error is given for both investigated weighting types. It can be seen that with increasing influence radius the error using the Gaussian weighting function increases but the error from the regularized type remains very small. This means that Eq. (23) is fulfilled with extremely high accuracy if the regularized weighting function is used.

The influence of the minimum nodal distance on the interpolation accuracy is investigated on the irregular set of nodes shown in Fig. 7 by changing the distance between node A and B. The influence radius is kept constant with D = 0.5 m. In Table 2 the obtained interpolation errors are shown. The table clearly indicates that the interpolation error by using the regularized weighting function is very small even if the nodal arrangement is strongly irregular. Additionally the maximum weighting function error at the supporting points and the approximated values by using

Table 1 Maximum numerical error at the nodes as a function of the influence radius

D	$\left\|\Phi_{i,G}^{MLS}(\mathbf{x}_j) - \delta_{ij}\right\|_{\max}$	$\left\|\Phi_{i,R}^{MLS}(\mathbf{x}_j) - \delta_{ij}\right\|_{\max}$
0.3 m	0.6%	$1.32 \cdot 10^{-4}$%
0.4 m	10.1%	$1.71 \cdot 10^{-5}$%
0.5 m	30.5%	$7.10 \cdot 10^{-6}$%
0.6 m	49.5%	$1.11 \cdot 10^{-5}$%
1.0 m	81.5%	$1.47 \cdot 10^{-5}$%

Table 2 Maximum numerical error as a function of the minimum nodal distance

d_{AB}/D	$\left\|\Phi_{i,G}^{MLS}(\mathbf{x}_j) - \delta_{ij}\right\|_{\max}$	$\left\|\Phi_{i,R}^{MLS}(\mathbf{x}_j) - \delta_{ij}\right\|_{\max}$	$\left\|w_{i,R}(\mathbf{x}_j) - \delta_{ij}\right\|_{\max}$	
			Numerical	Approximation
0.4	36.8%	$1.19 \cdot 10^{-5}$%	$3.81 \cdot 10^{-9}$	$3.81 \cdot 10^{-9}$
0.2	47.7%	$2.34 \cdot 10^{-6}$%	$6.24 \cdot 10^{-8}$	$6.24 \cdot 10^{-8}$
0.1	55.2%	$1.02 \cdot 10^{-5}$%	$9.97 \cdot 10^{-7}$	$1.00 \cdot 10^{-6}$
0.01	59.0%	$1.05 \cdot 10^{-3}$%	$8.26 \cdot 10^{-3}$	$1.00 \cdot 10^{-2}$
0.001	59.0 %	$1.05 \cdot 10^{-1}$%	$8.26 \cdot 10^{-1}$	-

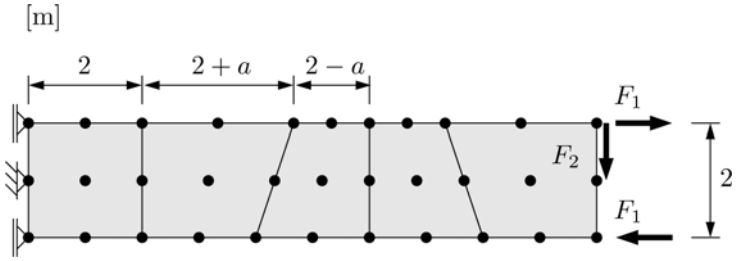

Fig. 8 Investigated distorted cantilever with Q9 mesh

Eq. (29) are shown in the table. It can be seen, that the approximated values agree very well with the numerical values. For $d_{AB}/D = 0.001$ the assumption in Eq. (28) is not valid and the approximation in Eq. (29) can not be used.

4.2 Cantilever under higher order displacement fields

Within this example the accuracy of the regularized weighting function embedded in a Galerkin method is investigated for higher order displacement fields as a function of increasing distortion of the nodal arrangement. In Fig. 8 the system with geometrical properties and boundary conditions is shown. Two different load cases have been investigated, first a moment load at the beam end represented by the load pair F_1, which leads to a quadratic displacement field, and second a single vertical load F_2 at the beam end, which results in a cubic displacement field. For comparison the investigated beam was discretized with four-node (Q4) and nine-node (Q9) iso-parametric finite elements. In Fig. 8 the Q9 discretization is shown exemplarily. For both investigated load cases the material was assumed to be linear elastic. The material properties are 3000 N/m^2 for the Young's modulus and $\nu = 0.0$ for the Poisson's ratio and the thickness was defined to be 0.1 m. For the system matrix computation Delaunay triangle background cells are used, which are spanned by three nodes. These triangles are computed automatically with the "Triangle" package (Shewchuk 1996), whereby a constrained Delaunay triangulation of a planar straight line graph (Fortune 1995) is assembled by defining the domain boundary as a number of segments with two nodes as endpoints. The numerical integration is carried out via a Gauss quadrature over 25 integration points per triangular background cell. This relatively high number of integration points are used to reduce the numerical errors from the integration procedure. The application of the boundary conditions by using the Gaussian weighting function was done via a weighting function blending (Most *et al.* 2004a), which is based on the blending technique in transition elements (Belytschko *et al.* 1995).

In Fig. 9 the obtained maximum nodal displacement errors for the first load case are shown as a function of increasing distortion a. By using the Q9 finite elements the analytical solution was obtained exactly for every distorted system. The meshless calculations with the quadratic base polynomial led to a very good agreement for the undistorted structure. The remaining deviations from the analytical solution are a result of the integration error. With increasing distortion the usage of the Gaussian weighting function results in an increasing error, whereby the application of the regularized type gives very good results even for stronger distortions. For the calculations using the bilinear base polynomial the same trend was observed, there the results from the regularized weighting function are slightly better than those obtained with the Q4 finite elements with bilinear

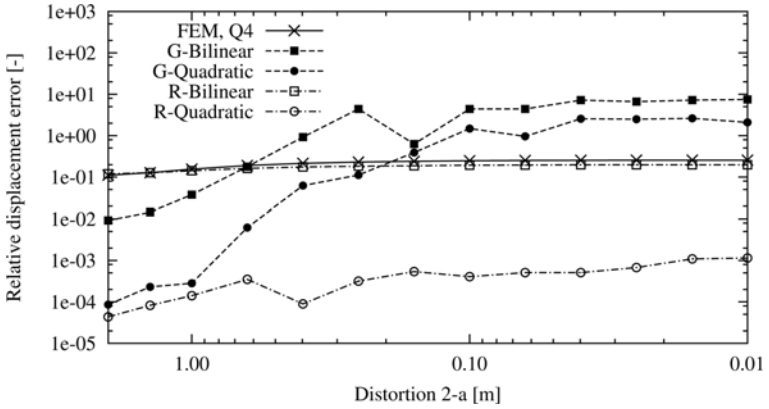

Fig. 9 Maximum nodal errors for a quadratic displacement field under increasing distortion obtained by using Gaussian (G) and regularized (R) weighting functions and bilinear and quadratic base polynomials

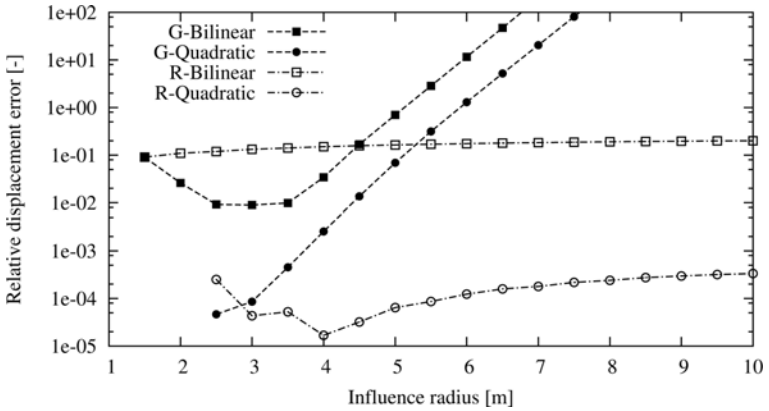

Fig. 10 Maximum nodal error for a quadratic displacement field for both weighting types depending on the influence radius *D*

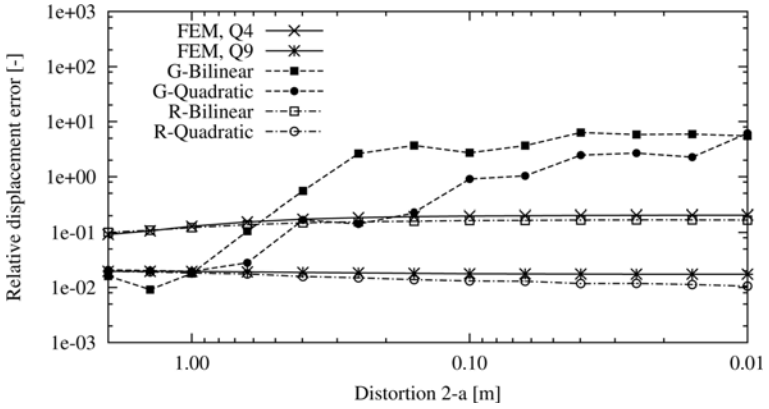

Fig. 11 Maximum nodal error for a cubic displacement field by increasing distortion

shape functions. The meshless simulations were carried out by taking D = 2.5 m for the bilinear base polynomial and D = 3.0 m for the quadratic polynomial. In Fig. 10 the influence of D on the displacement error is shown. The figure indicates, as already shown in the previous examples, that the results obtained with the regularized weighting type are almost independent of the influence radius size in strong contrast to those from the Gaussian weighting function.

In Fig. 11 the calculated displacement errors for the second load case are shown. The same trend as for the first load case was observed: the regularized weighting function leads to results which are almost independent of the distortion, whereby the Gaussian weighting types could not give sufficient results for strong distortions. The results obtained with the regularized function are slightly better than the finite element solutions with corresponding polynomial order.

4.3 Calculation of Mode-I stress intensity factors by Virtual Crack Extension

This example was chosen to investigate the convergence of the developed weighting function interpolation for a Mode-I problem from linear elastic fracture mechanics. For this purpose a quadrilateral panel with a horizontal central crack as shown in Fig. 12 was analyzed by calculating the Mode-I stress intensity factor by using the Virtual Crack Extension technique as presented in (Yang *et al.* 2001). As shown in Fig. 12 a uniform vertical stress was applied with $\sigma = 1.0 \cdot 10^6$ N/m^2. The material properties were taken as $E = 2.0 \cdot 10^{11}$ N/m^2 for the Young's modulus and $\nu = 0.3$ for the Poisson's ratio. The thickness was assumed with t = 1.0 m and plane strain condition was implied. For the numerical analysis different nodal discretizations were investigated and only one half of the plate was modeled by considering the symmetry of the system. In Fig. 12 the resulting nodal setup with boundary conditions is shown additionally for the coarsest grid of 5 × 9.

The analytical solution for this problem is given in (Tada *et al.* 1993) as $K_I = 4.72 \cdot 10^6$ N/$\sqrt{\text{m}}$. In Fig. 13 the obtained numerical errors for the FEM and MLS calculations from the analytical solution are shown. For the FEM calculations four-node (Q4) quadrilateral 2D-solid elements with regular node distribution have been taken. The MLS calculations were carried out by using the

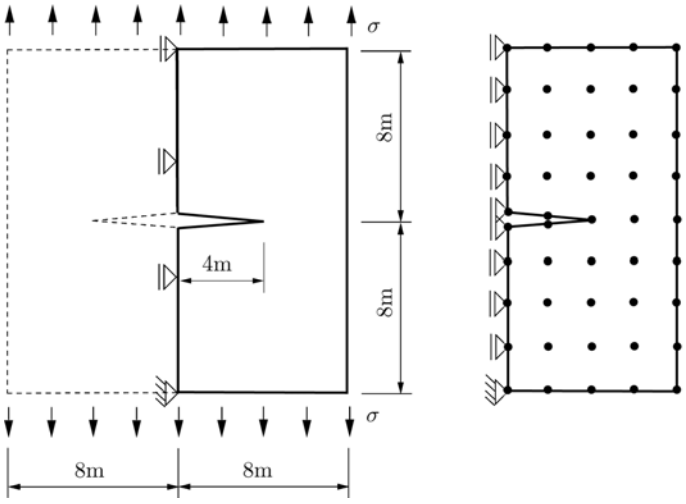

Fig. 12 Mode-I fracture: square plate with horizontal crack and nodal discretization

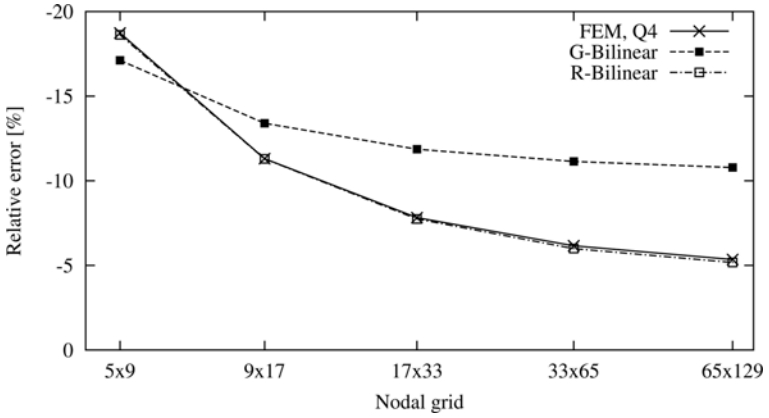

Fig. 13 Numerical error for the Mode-I stress intensity factor obtained by using Gaussian (G) and regularized (R) weighting functions with bilinear base polynomials

Gaussian and the new regularized weighting function with a regular nodal grid and an unique influence radius $D = 2d_{\min}$, where $d_{\min}$ is the minimal nodal distance. The boundary conditions for the Gaussian weighting function are applied again by using the weighting function blending technique (Most *et al.* 2004a). The numerical integration was done again using Delaunay triangles spanned by three nodes each having 25 Gauss integration points. The virtual crack extension length was assumed with $\Delta a = 10^{-4}\, d_{\min}$. The results for the Q4 elements show excellent agreement with these obtained by (Yang *et al.* 2001) (5×9 nodes: –18.6%, 9×17 nodes: –11.2%). The numerical prediction of K_I using the regularized weighting function gives similar results as with finite elements. If the Gaussian weighting function is used, the convergence is much less than with the regularized weighting function or with finite elements. This shows analogous to the previous example the more robust character of the new weighting function.

All of the presented results for this example were carried out with the standard interpolation functions. Better results for this problem with crack tip singularity can be obtained for finite elements with special eight-node crack tip elements (Barsoum 1974) and for the MLS interpolation by using an enriched based polynomial according to (Fleming 1997)

$$\mathbf{p}^T(\mathbf{x}) = \left(1 \;\; x \;\; y \;\; xy \;\; \sqrt{r}\cos\frac{\theta}{2} \;\; \sqrt{r}\sin\frac{\theta}{2} \;\; \sqrt{r}\sin\frac{\theta}{2}\sin\theta \;\; \sqrt{r}\cos\frac{\theta}{2}\sin\theta\right) \tag{33}$$

where r and θ are the polar coordinates with respect to the crack tip. For the sake of comparability of the finite element and the MLS calculations these extensions were not applied and only the standard interpolation functions were used in this paper.

5. Conclusions

In this paper a new regularized weighting function for the Moving Least Squares interpolation is presented. In contrast to common weighting function types, this new formulation enables the fulfillment of the interpolation condition with very high accuracy. Thus the essential boundary conditions are fulfilled automatically and no additional numerical effort is necessary for the

application in a Galerkin method. Furthermore the results obtained with the new weighting function are very stable with respect to the modification of the influence radius. Huge distortions of the nodal arrangement does not influence the results significantly. Thus the new interpolation can be applied directly for irregular sets of nodes.

Due to the almost vanishing derivatives of the weighting function on the influence domain boundaries, the obtained interpolation shows approximative C^1 and C^2 continuity, which enables an efficient application for response surface methods or data interpolation procedures.

The main problem for the application of the MLS interpolation is solved with this new weighting function type, which makes the MLS interpolation more attractive especially within a Galerkin method. This will be clear by pointing out, that the choice of the base polynomial is arbitrary, thus the accuracy can be increased by choosing higher order polynomials.

Acknowledgements

This research has been supported by the German Research Council (DFG) through Collaborative Research Center 524, which is gratefully acknowledged by the authors.

References

Barsoum, R. (1974), "Application of quadratic isoparametric finite elements in linear elastic fracture mechanics", *Int. J. Fracture,* **10**, 603-605.

Belytschko, T., Krongauz, Y., Organ, D., Fleming, M. and Krysl, P. (1996), "Meshless methods: An overview and recent developments", *Comput. Meth. Appl. Mech. Eng.*, **139**, 3-48.

Belytschko, T., Lu, Y. and Gu, L. (1994), "Element-free Galerkin methods", *Int. J. Numer. Meth. Eng.*, **37**, 229-256.

Belytschko, T., Organ, D. and Krongauz, Y. (1995), "A coupled finite element-element-free Galerkin method", *Int. J. Comput. Mech.*, **17**, 3057-3080.

Chen, J.-S., Wu, C.-T., Yoon, S. and You, Y. (2001), "A stabilized conforming nodal integration for Galerkin mesh-free methods", *Int. J. Numer. Meth. Eng.,* **50**, 435-466.

Fleming, M. (1997), "The Element-free Galerkin method for fatique and quasi-static fracture", Ph.D. Thesis, Northwestern University, Evanston, Illinois.

Fortune, S. (1995), *Computing in Euclidean Geometry*, Vol. **1** of *Lecture Notes Series on Computing*, 193-233, Du, D.-Z. and Hwang, F.K.

Häussler-Combe, U. (2001), "Elementfreie Galerkin-Verfahren: Grundlagen und Einsatzmöglichkeiten zur Berechnung von Stahlbetontragwerken", Habilitation-Thesis, University of Karlsruhe, Germany.

Karutz, H. (2000), "Adaptive Kopplung der Elementfreien Galerkin-Methode mit der Methode der Finiten Elemente bei Rissfortschrittsproblemen", Ph.D. Thesis, Ruhr-Universität Bochum, Germany.

Lancaster, P. and Salkauskas, K. (1981), "Surfaces generated by moving least squares methods", *Mathematics of Computation.,* **37**, 141-158.

Liew, K.M., Huang, Y.Q. and Reddy, J.N. (2003a), "Moving least squares differential quadrature method and its application to the analysis of shear deformable plates", *Int. J. Numer. Meth. Eng.,* **56**, 2331-2351.

Liew, K.M., Huang, Y.Q. and Reddy, J.N. (2003b), "Vibration analysis of symmetrically laminated plates based on FSDT using moving least squares differential quadrature method", *Comput. Meth. Appl. Mech. Eng.,* **192**, 2203-2222.

Liew, K.M., Huang, Y.Q. and Reddy, J.N. (2004), "Analysis of general shaped thin plates by the moving least-squares differential quadrature method", *Finite Elements in Analysis and Design,* **40**, 1453-1474.

Most, T. and Bucher, C. (2003), "Moving Least Squares"-elements for stochastic crack propagation simulations

coupled with stochastic finite elements. In A. Der Kiureghian, S. Madanat, and J. Pestana (Eds.), *Proc. 9th Int. Conf. Appl. of Stat. and Prob. Civil Eng.,* San Francisco, California, July 6-9. Rotterdam: Balkema.

Most, T., Unger, J. and Bucher, C. (2004a), "Stochastic crack growth simulation in R/C structures by means of meshless methods", In C. Bucher and T. Takada (Eds.), *Proc. of the 1st Workshop on Performance Evaluation of Existing Structures,* Weimar, December 9-10, 2004.

Most, T., Unger, J.F. and Bucher, C. (2004b), "Cohesive discrete crack modeling using Virtual Crack Extension technique within the Natural Neighbor Galerkin Method", *Comput. Struct.*, Submitted for publication.

Shewchuk, J. (1996), "Triangle: A two-dimensional quality mesh generator and Delaunay triangulator", Technical Report, School of Computer Science, Carnegie Mellon University. download: http://www.cs.cmu.edu/quake/triangle.html.

Sukumar, N., Moran, B. and Belytschko, T. (1998), "The Natural Element Method in solid mechanics", *Int. J. Numer. Meth. Eng.*, **43**, 839-887.

Tada, H., Paris, P. and Irwin, G. (1993), *The Stress Analysis of Cracks Handbook.* Hellertown, Pennsylvania: Del Research Corporation.

Unger, J.F., Most, T., Bucher, C. and Könke, C. (2004), "Adaptation of the natural element method for crack growth simulations", In P. Neittaanmäki, T. Rossi, K. Majava, and O. Pironneau (Eds.), *Proc. 4th European Congress on Comp. Mechanics in Appl. Sciences and Eng.*, Jyväskylä, Finland, July 24-28.

Yang, Z., Chen, J. and Holt, G. (2001), "Efficient calculation of stress intensity factors using virtual crack extension technique", *Comput. Struct.*, **79**, 2705-2715.

Appendix A: Interpolation error of regularized weighting function

Eq. (25) and Eq. (26) lead to the following formulation

$$w_R(d_i) = \frac{\left(\left(\frac{d_i}{D}\right)^2 + \varepsilon\right)^{-2} - (1+\varepsilon)^{-2}}{\sum_{j=1}^{m}\left[\left(\left(\frac{d_j}{D}\right)^2 + \varepsilon\right)^{-2} - (1+\varepsilon)^{-2}\right]} \tag{34}$$

If we assume

$$\varepsilon << 1; \quad \left(\frac{d_{\min}}{D}\right)^2 >> \varepsilon \tag{35}$$

we can approximate

$$\sum_{j=1}^{m}\left[\left(\left(\frac{d_j}{D}\right)^2 + \varepsilon\right)^{-2} - (1+\varepsilon)^{-2}\right] \approx \varepsilon^{-2} - 1 + \sum_{j=1;\, j\neq i}^{m}\left[\left(\frac{d_j}{D}\right)^{-4} - 1\right] \approx \varepsilon^{-2} \tag{36}$$

by considering the fact, that the distance d_i for the support point itself is equal to zero. Under consideration of

$$\left(\left(\frac{d_i}{D}\right)^2 + \varepsilon\right)^{-2} \leq \left(\left(\frac{d_{\min}}{D}\right)^2 + \varepsilon\right)^{-2} \tag{37}$$

where $d_{\min}$ specifies the minimum distance between two arbitrary nodes, and of Eq. (36) we obtain for the maximum error of the weighting function

$$\begin{aligned} \left|w_i(\mathbf{x}_j) - \delta_{ij}\right|_{\max} &\approx \left[\left(\left(\frac{d_{\min}}{D}\right)^2 + \varepsilon\right)^{-2} - (1+\varepsilon)^{-2}\right] \cdot \varepsilon^2 \\ &\approx \left(\left(\frac{d_{\min}}{D}\right)^{-4} - 1\right) \cdot \varepsilon^2 \end{aligned} \tag{38}$$

Using the simpler formulation from Eq. (26) we obtain under considering Eq. (36) and Eq. (37) the same

expression as given in Eq. (38)

$$\left|\tilde{w}_i(\mathbf{x}_j) - \delta_{ij}\right|_{\max} \approx \left(\left(\frac{d_{\min}}{D}\right)^{-4} - 1\right) \cdot \varepsilon^2 \tag{39}$$

Appendix B: Values of the first and second derivatives of the regularized weighting function on the boundary of the influence domain

The value of the first derivative of the weighting function on the influence boundary ($d = D$) reads

$$\frac{\partial \tilde{w}_R(d = D)}{\partial d} = -\frac{4}{D}\frac{(1+\varepsilon)^{-3}}{\varepsilon^{-2} - (1+\varepsilon)^{-2}} \tag{40}$$

By assuming

$$\varepsilon << 1 \tag{41}$$

we obtain

$$\frac{\partial \tilde{w}_R(d = D)}{\partial d} \approx 4\varepsilon^2 \frac{1}{D} \tag{42}$$

For the second derivative we obtain analogically

$$\frac{\partial^2 \tilde{w}_R(d = D)}{\partial^2 d} = \frac{\frac{24}{D^2}(1+\varepsilon)^{-4} - \frac{4}{D^2}(1+\varepsilon)^{-3}}{\varepsilon^{-2} - (1+\varepsilon)^{-2}} \tag{43}$$

and

$$\frac{\partial^2 \tilde{w}_R(d = D)}{\partial^2 d} \approx 20\varepsilon^2 \frac{1}{D^2} \tag{44}$$